Journal of Ceramic Processing Research. Vol. 22, No. 5, pp. 590~596 (2021)
(Received 20 April 2021, Received in revised form 30 August 2021, Accepted 11 September 2021)
https://doi.org/10.36410/jcpr.2021.22.5.590

J O U R N A L O F
Ceramic Processing Research

Microstructural evolution and mechanical properties of TiC-Mo_2C-WC-Ni multi-component powder by high energy ball milling

Jeong-Han Lee[a,b] and Hyun-Kuk Park[a,*]
[a]*Korea Institute of Industrial Technology (KITECH), Smart Mobility Materials and Components R&D Group, 6, Cheomdan-gwagiro 208-gil, Buk-gu, Gwang-Ju, 61012, Korea*
[b]*Chonnam National University, Materials Science & Engineering, 77, Yong-bongro, Buk-gu, Gwang-ju, 61186, Korea*

The widespread use of TiC-based cermets as cutting tools, thin-film, ultracapacitors, nozzles, and bearings is primarily due to exhibit combination of excellent mechanical properties such as low density, high hardness, and stiffness. The TiC cermets were synthesized by high energy ball milling, which includes binder metal (Ni), carbides (WC and Mo_2C), wherein the present study focus on the relationship between the core-rim structure, phase constitution, and mechanical properties. Here, using in situ TEM, we clearly observed the behavior of adjacent core-rim formation from the solid-phase reaction with grain refinement of the TiC phase control of both the milling time and lattice formation. Also, we proposed that mechanically alloyed core-rim structure can affect oxidation resistance of TiC-Mo_2C-WC-Ni cermets strongly related to activation energy attributed to TiC particle size. The mechanical properties of TiC-Mo_2C-WC-Ni cermets suggest the hardening effect is not considered only grain refinement, but rather is solid solution strengthening and particle-dispersion hardening. The present study paves the relation to the formation behavior of both TiC hard phase and core-rim structure due to the mechanical powder synthesis of novel TiC-based cermets.

Keywords: Titanium carbide; metal matrix composites, mechanical alloying, core-rim structure, micro-hardness

Introduction

TiC-based cermets are widely used for engineering materials and in cutting tools because of their high hardness/strength, good wear/corrosion resistance, chemical inertness, and high thermal stability [1-4]. Commercial TiC-based cermets generally contain refractory carbides (Mo_2C, TaC, and WC) and metallic binders (Co, Fe, and Ni) in order to enhance several performance such as consolidation, fracture toughness, and wear resistance [5-10]. To challenge the poor sinterability of TiC, that Mo_2C and WC can be added to it to increase its wettability to the Ni binder [11].

TiC-based cermets containing Mo_2C and WC, they have specific microstructures with respect to the core (TiC) and rim (Ti, Mo or W)C. These structures are formed by a solid-state diffusion process (inner-rim) and dissolution-reprecipitation (outer-rim) mechanism, resulting in a finer hard phase as the TiC core hindering the coarsening grains [12-15].

The grain refinement effect of TiC-cermets can be boosted by mechanical alloying (MA) through the solid-state powder processing of particles with high-energy ball milling [16-19]. The non-equilibrium phases such as prealloyed inter-particles, which are considered supersaturated solid solutions [20], can form a component similar (e.g., mechanically bonded brittle/brittle component) to the core–rim structure. H. Hosokawa et al. reported [21] the microstructural evolution and change in the chemical component of Ti-Mo-Ni-C powders from 1 to 700 h mechanical milling; thereby the TiC particles consisted of fine grains about 5 nm with those for the core–rim structure (Ti, Mo)C.

However, only few studies have been reported on the variation in mechanical properties depending on their lattice structure and phase states (intermetallic compounds, solid solutions, and amorphous) for TiC-Mo_2C-WC-Ni cermet powders during the milling process. Hence, it is still worth discussing the thermal behaviour of fine particles for pre-alloyed mechanically after the milling process. Bouleghlem et al. [22] reported the effect of thermal reactions and diffusions of WC-TiC-TaC-NbC-Co mixture powder, wherein sintered components ((Ti, W)C/WC) were caused by solution-reprecipitation phenomena. Therefore, the purpose of this study is to understand the effects of microstructure and the mechanical properties of TiC-15Mo_2C-10WC-9.6Ni alloyed powders by means of mechanically bonded components between (Ti, Mo)C and (Ti, W)C. In particular, significant attention was paid to investigate the structural evolution depending on the milling times, that is, phase constitution, lattice parameter, micro strain, and thermal decomposition.

*Corresponding author:
Tel : +82 62 600 6270
Fax: +82 62 600 6149
E-mail: hk-park@kitech.re.kr

Experimental

TiC (≤ 2.0 μm, Alfa Aesar.), Mo_2C (≤ 44.0 μm, Alpha Ltd.), WC (≤ 0.5 μm, Taegutec.), and Ni (≤ 44.0 μm, Alpha Ltd.) powders were used as raw materials. These powders were mechanically alloyed by planetary (high-energy) ball milling with WC balls under a ball-to-powder ratio of 2:1. The milling process was performed for 6, 12, 24, and 48 h in ethanol media at 300 RPM. The phase constitution and the lattice parameters of TiC-15Mo_2C-10WC-9.6Ni alloyed powders were investigated with respect to the milling time using X-ray diffraction (XRD) with Cu Kα radiation (λ = 0.154 nm). In addition, the average crystallite size and microstrain of the TiC-15Mo_2C-10WC-9.6Ni alloyed powders were measured using the Williamson Hall (W-H) method in Eq. (1)-(3) [23].

$$D=\frac{k\lambda}{\beta_{hkl}\cos\theta},\ \varepsilon=\frac{\beta_{hkl}}{4\tan\theta} \tag{1}$$

$$\beta_{hkl}=\left(\frac{k\lambda}{D\cos\theta}\right)+4\varepsilon\tan\theta \tag{2}$$

$$\beta_{hkl}\cos\theta=\left(\frac{k\lambda}{D}\right)+4\varepsilon\sin\theta \tag{3}$$

where D is the crystallite size, k is Scherre's constant (0.9) with shape factor, and λ is the wavelength of Cu Kα radiation. The instrumental broadening is expressed as the β_{hkl} of the corrected value, which induces the intrinsic micro strain (ε). The mechanical alloyed powders were observed for their thermal stability and decomposition up to 1000 °C at a heating rate of 10 °C/min using a TGA-DTA (Thermogravimetric Analysis-Differential Thermal Analysis) method. The microstructural evolution of TiC-15Mo_2C-10WC-9.6Ni alloyed powders by mechanical milling time was investigated by TEM analysis considering the crystallinity according to their diffraction pattern.

The mechanical properties, such as microhardness and elastic modulus, of TiC-15Mo_2C-10WC-9.6Ni alloyed powders were evaluated by nanoindentation with a load of 20 gf ($HV_{0.02}$) under the Sneddon stiffness equation [24] and contact parameters. Then, the microhardness can be calculated as shown in Eq. (4):

$$H=\frac{P}{A} \tag{4}$$

where P is the peak loading and A is the projected contact area. The elastic modulus can be expressed by Eq. (5)-(6):

$$A=f(h_c),\ h_c=h_{max}-\varepsilon_i\left(\frac{P}{S}\right) \tag{5}$$

$$E_r=\frac{1}{\beta}\cdot\frac{\sqrt{\pi}}{2}\cdot\frac{S}{\sqrt{A}} \tag{6}$$

where h_c is the contact depth of indentation, β is the indenter geometry shape factor (1.012), and ε_i is the intercept factor (0.75).

Results and Discussion

Fig. 1 shows the XRD patterns of TiC-15Mo_2C-10WC-9.6Ni alloyed powders for different times. For a milling time of 6 (Fig. 1(a)) to 48 h (Fig. 1(e)), the crystalline peaks gradually decreased with increasing milling time, implying a refinement of the grain size. Notably, from 12 h (Fig. 1(c)) milling, (Ti, Mo)C_{1-x} [25] and (Ti, W)C_{1-x} [26] were observed though shifting of initial TiC peak, i.e. 35.92° to 35.99° and 60.65 to 60.53°. Therefore, it is observed that the WC and Mo_2C peaks disappeared after the 12 h milling, wherein the corresponding supersaturated solid solutions were formed. These non-stoichiometric carbides were considered to

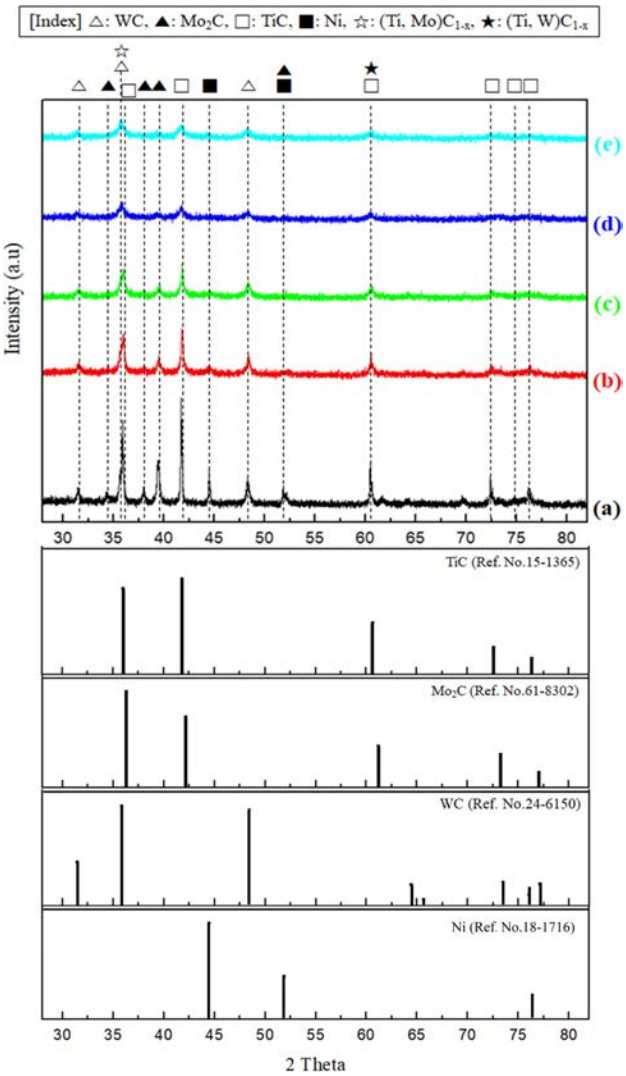

Fig. 1. XRD patterns of TiC-15Mo_2C-10WC-9.6Ni (wt.%) alloy powder processed by high energy ball milling process: (a) raw powder, (b) 6 h milled, (c) 12 h milled, (d) 24 h milled, and (e) 48 h milled.

be products of severe agglutinated or embedded fine particles by mechanical alloying. After 48 h of milling time, most peaks completely broadened, except for those indicating supersaturated solid solutions, in which the particles were characterised as nanoscale.

Fig. 2 presents the variation in the crystallite sizes of TiC, Mo_2C, WC, and Ni as a function of milling time, calculated by Eq. (1)-(3). The mean crystallite sizes of TiC, Mo_2C, and WC particles from 0 to 12 h were significantly decreased by dominated cold welding and fracturing during of compounds or supersaturated solid solutions were distributed significantly refined from 0 to 12 h (approximately 426 to 14 nm), whereas on further milling, the particle size could not be characterized because they completely broadened the peaks with very fine particles or amorphization.

The variation in lattice parameter and microstrain of candidates capable of forming the core–rim structures in TiC particles were obtained from XRD patterns as a function of milling time, as shown in Fig. 3. It was

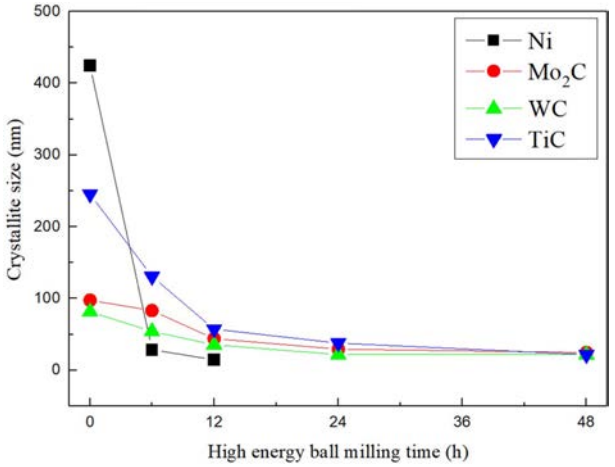

Fig. 2. Variation of average diffracting crystallite size of TiC, Mo_2C, WC, and Ni elements by the milled time.

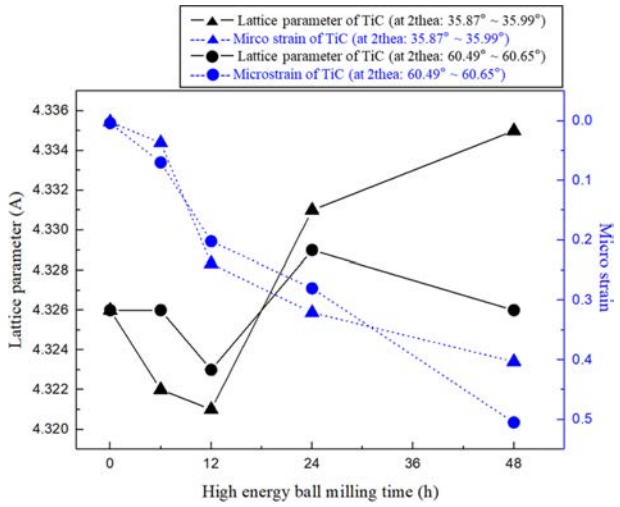

Fig. 3. Lattice parameter versus micro strain for TiC in TiC-15Mo_2C-10WC-9.6Ni (wt.%) alloy powders.

clear that the microstrain increased with severe plastic deformation [27] induced by the phase transformation from TiC to non-stoichiometric carbides (e.g., (Ti, Mo)C_{1-x} and (Ti, W)C_{1-x}) with increasing milling time. This heavy plastic deformation induces strong lattice distortion, causing lower crystallinity with disorder in the atomic arrangement [28]. On the other hand, the lattice parameter had undergone an increase or decrease during the three stages.

In the early stage of milling from 0 to 12 h, the decrease in the lattice parameters of TiC particles were caused by the compressive stress between neighbouring atoms with severe atomic collision [29]. In the second stage of milling from 12 to 24 h, an increase in the lattice parameters was observed. This was attributed to the tendency to precipitate the molybdenum and tungsten atoms by accumulated defects such as irregular strain and potential energy within the lattice of the super-saturated solid solutions [30]. Therefore, the solid solutions were subjected to tensile stress due to the influence of these two internal energies, resulting in an increase in the lattice parameter. The variation in lattice parameters was measured using TiC (4.321 Å at 35.99°) to (Ti, Mo)C_{1-x} (4.331 Å at 35.90°) and TiC (4.323 Å at 60.58°) to (Ti, W)C_{1-x} (4.329 Å at 60.49°), respectively. In the final stage of milling from 24 to 48 h, the difference in the lattice behaviour of the two solid solutions was clearly observed. In (Ti, W)C_{1-x}, there is an increased tendency of precipitation of the tungsten atoms due to the accumulated compressive stress causing the lattice collapse [31] of the solid solution. As a result, the Ti-C and W-C bonds were characterised as stable phases, that is, TiC and WC. This lattice behaviour was confirmed by the recovery of the initial TiC lattice parameter (4.326 Å at 60.54°). However, in (Ti, Mo)C_{1-x}, it was considered that the lattice distortion with an increase in the lattice parameter (4.331 Å to 4.335 Å) was subjected to continuous compressive stress while maintaining their solid solution structure.

Fig. 4 shows the TGA-DTA results for TiC-15Mo_2C-10WC-9.6Ni alloyed powders according to the milling time. In the DTA, exothermic reactions were observed at 220 °C (at 12, 24, 48 h milled), 246 °C (at 6 h milled), 396 °C (non-milled), and 482 °C (non-milled) in accordance with the equilibrium state of the powders. The mechanical alloying helps generate new interfaces, on the surface of particles that try to break, encouraging direct contact between the reactants in the inter-particles. Moreover, it is thought that the early stage reaction for the high reactivity interface reduces reaction onset temperatures. Notably, the metastable phases of the mechanically alloyed powders were revealed to have broad exothermic peaks at relatively low temperatures [32], which were caused by the energy release during heating due to early surface crystallisation, grain growth, and structural relaxation with internal stress [33].

In the TGA, there was oxidative decomposition of

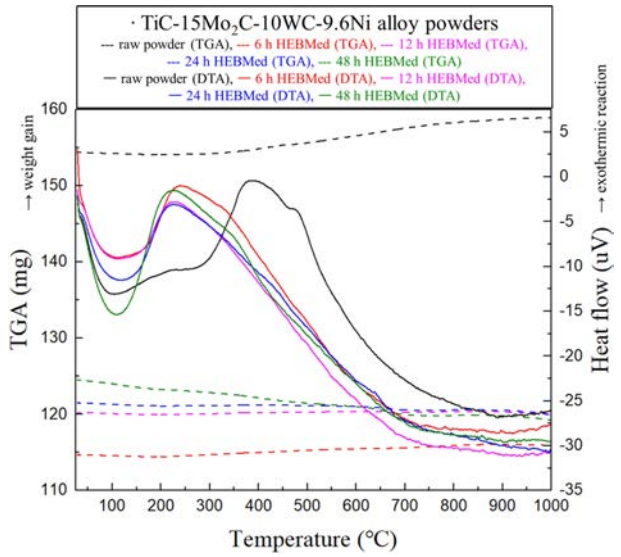

Fig. 4. TGA-DTA curves in TiC-15Mo_2C-10WC-9.6Ni alloy powders by the milled time.

the milled powders from 0 to 6 h with traces of weight gain. It was evident that the TiC particle oxidation transformed into oxycarbide ($TiO_{1-x}C_x$) and anatase (TiO_2) [34]. The oxidation behaviour of TiC-15Mo_2C-10WC-9.6Ni alloyed powders decreased significantly with increasing particle size. Furthermore, Boatemaa et al. reported [35] that the activation energy is related strongly to the TiC particle size; thereby the energy distribution ranged from 243 ± 42 (140 μm) to 122 ± 24 kJ mol^{-1} (0.05 μm). Therefore, it can be concluded that the core–rim structures by mechanical bonding could contribute to the improvement of the oxidation resistance of TiC. Alternatively, the powders milled from 12 to 48 h exhibit weight loss behaviour, wherein the early thermal decomposition [36] causes the breaking apart of atom bonds for metastable phases.

Fig. 5 demonstrates the microstructural evolution with an elemental distribution for TiC-15Mo_2C-10WC-9.6Ni alloyed powders. After milling, the particles become significantly decrease in size and granularity in morphology, specifically incorporated towards the matrix particle in large aggregates. While raw powders deformed after 12 h of milling (*see* Fig. 5(a) to Fig. 5(c)), the TiC particle (matrix) size decreased significantly between the Mo, W, and Ni particles. With continued deformation, the agglomerates become cold-welded and get work-hardened towards fragmentation to conduct a fragile flake. After 24 h milling (*see* Fig. 5(d)), the TiC-based agglomerates consisted of a high concentration of Mo and W, in which the Ni-enriched regions were embedded in the matrix. Additional milling takes the powder more homogeneous while maintaining the morphology of the granules, in which particles attain a saturation level, due to the accumulation of strain energy. Thus, after 48 h milling (*see* Fig. 5(e)), it was observed that the W particles were separated compared to the

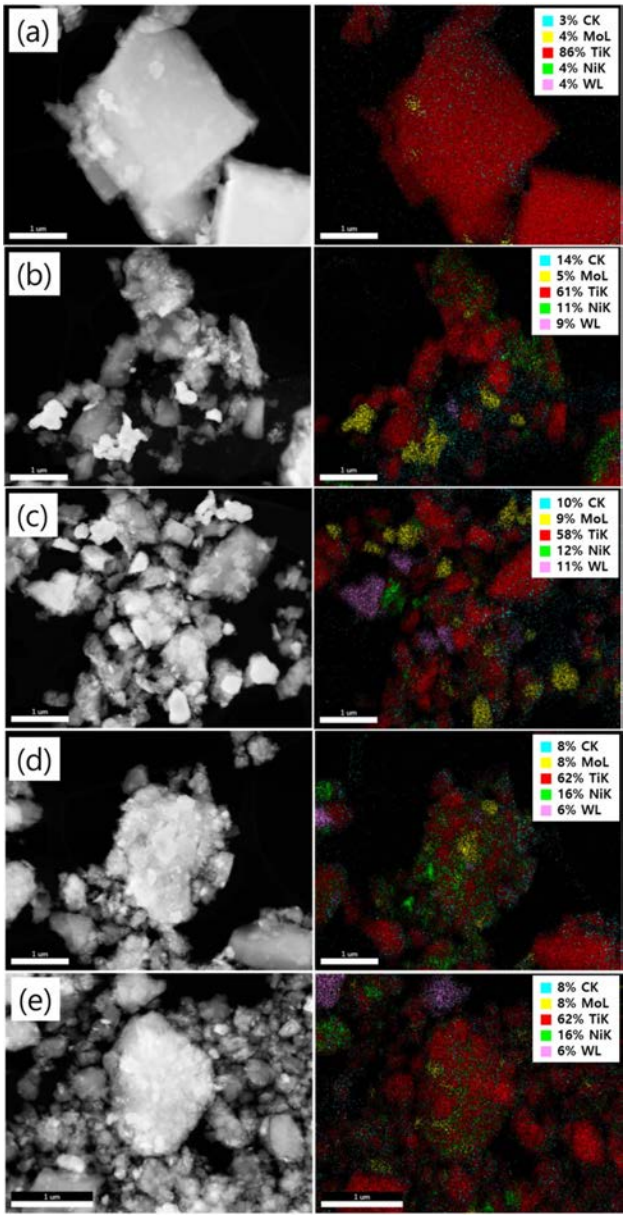

Fig. 5. STEM-DF images and EDS-mapping of TiC-15Mo2C-10WC-9.6Ni (wt.%) alloy powders processed by high energy ball milling process: (a) raw powder, (b) 6 h milled, (c) 12 h milled, (d) 24 h milled, and (e) 48 h milled.

agglomerates of the 24 h milling. In particular, it was confirmed that the tungsten particles cause precipitation behaviors consistent with the lattice structural evolution obtained from the XRD results.

The HR-TEM analysis and SAED patterns of the TiC-15Mo_2C-10WC-9.6Ni alloyed powders are shown in Fig. 6. The BF images in Fig. 6(a) show the typical SAED pattern for the TiC matrix corresponding to the d-spacing (2.497 Å) and (111) plane. However, Fig. 6(b), shows intermetallic compounds such as (Ti, Mo)C_{1-x} (JCPDS; 61-8347) and (Ti, W)C_{1-x} (JCPDS; 07-7553) consisting of nanocrystallines before the phase transition to the supersaturated solid solution. These intermetallic

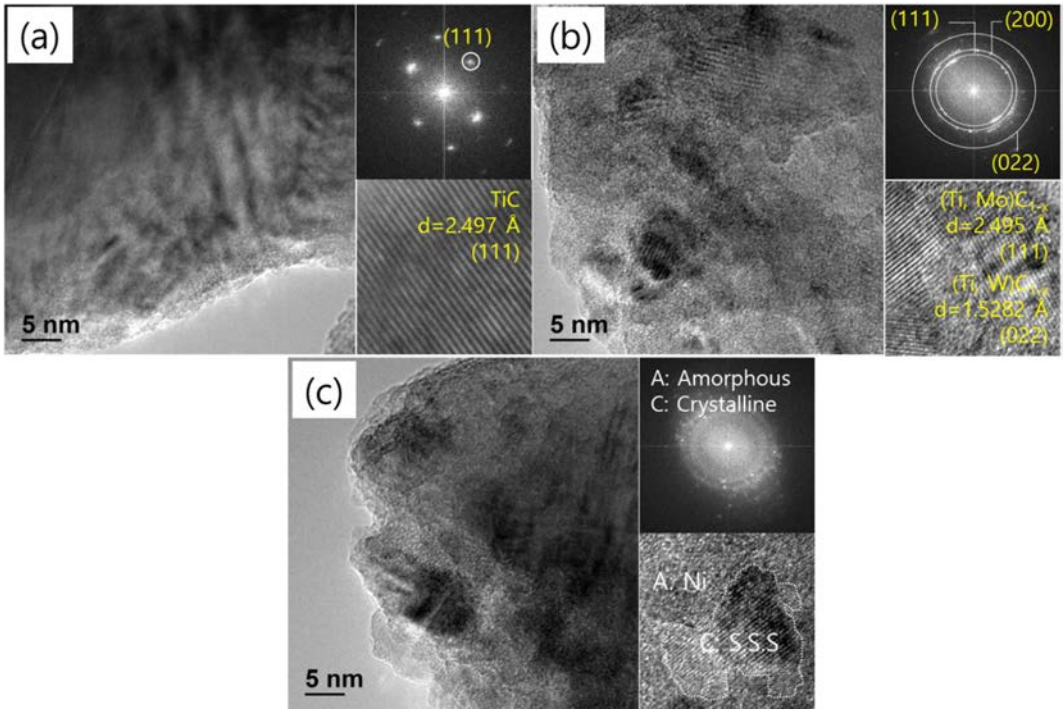

Fig. 6. HR-TEM images and their diffraction patterns of TiC-15Mo_2C-10WC-9.6Ni (wt.%) alloy powders processed by high energy ball milling process: (a) raw powder, (b) 12 h milled, and (c) 48 h milled.

compounds were preferentially oriented on the (111) and (022) planes and the d-spacing values consistent with the JCPDS information were investigated. In particular, it was concluded that Mo_2C could be advantageous for the formation of intermetallic compounds because Mo_2C (-17.6 kJ/mol [37]) has a lower value than WC (-35.1 kJ/mol [37]) in terms of their formation enthalpy for TiC. Fig. 6(c) shows the simultaneous nucleation relevant to partial amorphisation [38]. Corresponding to the diffraction pattern, the nanocrystalline was distributed within the Debye diffraction ring pattern. These nanocrystallines may be considered as molybdenum and tungsten dissolved into the TiC matrix [13], transformed into a supersaturated solid solution. Furthermore, the Ni particle was transformed from a crystalline to an amorphous phase. It was estimated that there was no crystallinity for Ni; therefore, XRD peaks and TEM diffraction data were not detected.

Fig. 7 shows the mechanical properties of TiC-15Mo_2C-10WC-9.6Ni alloyed powders, and Table 1 shows the average values of their nanohardness and elastic modulus. The 6 h milled specimen exhibited the highest nanohardness value (approximately 4.07 GPa), whereas the 12 h milled specimen had the lowest value (approximately 3.50 GPa). The hardening effect was estimated by the grain-boundary strengthening of TiC grains and the work-hardening of particles during cold-welding of the milling process [38]. However, the mechanical properties after 12 h of milling could be determined by the inner rim and the phase state adjacent to the Ni binder of TiC grains. In the 12 h

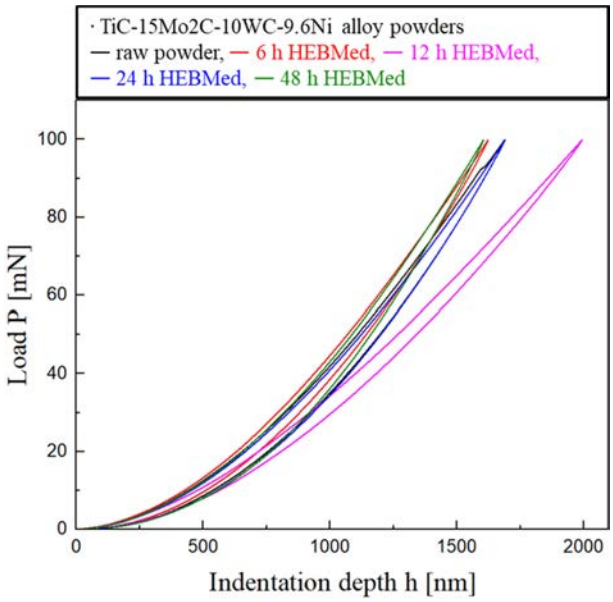

Fig. 7. Nanoindentation load-displacement curves of TiC-15Mo_2C-10WC-9.6Ni (wt.%) alloy powders.

milled specimen, the Mo_2C (~19 GPa) and WC (~22 GPa) of the inner-rim phases have relatively low intrinsic hardness values compared to TiC (~32 GPa). This factor deteriorates the hardness of the TiC-core, which interferes with the crack propagation caused by a difference in interfacial energy [39]. On the other hand, after 24 h of milling, there is a tendency for the hardness value (~3.95 to 4.12 GPa) to increase. This hardening behaviour was considered to be due to the

Table 1. Average and standard deviation (SD) of nanohardness and elastic modulus implemented from nanoindentation tests.

Milled time	Nanohardness / GPa		E_r / GPa	
	Average	SD	Average	SD
raw powder	4.07	0.06	194	0.07
6 h milled	4.42	0.07	220	0.07
12 h milled	3.50	0.05	144	0.06
24 h milled	3.95	0.07	192	0.07
48 h milled	4.12	0.07	209	0.08

solid solution strengthening effect [40] of the super-saturated TiC core–rim structures and the Ni particle-dispersion hardening in an amorphous structure [41].

Conclusion

The present study was dedicated to investigating the development of the core-rim structure that affects oxidation resistance and mechanical properties of TiC matrix in TiC-Mo_2C-WC-Ni cermets synthesized by high-energy ball milling followed by mechanical alloying. A summary of the conclusions follows:

(1) The core-rim structures (Ti, Mo)C_{1-x} and (Ti, W)C_{1-x} were formed with embedded fine particles after 12 h milling. The structural evolution of TiC with a variation of lattice parameter is revealed that solid solutions were subjected to tensile stress due to the influence of these two internal energies, whereas the compressive stress causing the lattice collapses of the solid solution.

(2) The core-rim structures attributed to mechanical alloying contribute to improving the oxidation resistance of TiC particles because reduces the distribution of activation energy for oxidation, thereby cores and TiC bonding could be suppressing grain growth.

(3) The microstructural evolution of TiC-15Mo_2C-10WC-9.6Ni alloyed powders revealed the formation of a nanocrystalline supersaturated solid solution and amorphization of the binder phase in accordance with severe plastic deformation within the agglomerated TiC-based matrix.

(4) The mechanical properties of the hardening effect of mechanically alloyed powders were closely related to several factors such as grain-boundary strengthening, work-hardening, solid-solution strengthening, and particle-dispersion hardening, in which the highest hardness value was approximately 4.42 GPa (6 h milled powder).

Acknowledgments

This study has been conducted with the support of the Korea Institute of Industrial Technology as “Development of Core Technologies for a Smart Mobility (KITECH JA-21-051)”.

References

1. A. Jam, L. Nikzad, and M. Razavi Ceram. Int. 43[2] (2017) 2448-2455.
2. Y. Yanaba, T. Takahashi, and K. Hayashi J. Jpn. Soc. Powder Metallur. 51[5] (2004) 374-384.
3. J. Jung and S. Kang, Acta Mater. 52[6] (2004) 1379-1386.
4. A. Rajabi, M. J. Ghazali, and A. R. Daud, Mater. Des. 67 (2015) 95-106.
5. S. Lemboub, S. Boudebane, F.J. Gotor, S. Haouli, S. Mezrag, S. Bouhedja, G. Hesser, H. Chadli, and T. Chouchane, Int. J. Refract. Met. Hard Mater. 70 (2018) 84-92.
6. N. Wu, F. Xue, H. Yang, H. Zhou, Y. Li, G. Li, and F. Luo, Mater. Today Comm. 25 (2020) 101311.
7. J. Pornbacher, H. Leitner, P. Angerer, T. Wojcik, S. Marsoner, and G. Ressel, Mater. Charact. 156 (2019) 109880.
8. I.J. Shon, J. Ceram. Process. Res. 17[8] (2016) 789-794.
9. I.J. Shon, J. Ceram. Process. Res. 17[5] (2016) 507-512.
10. B.W. Kwak, B.S. Kim, and I.J. Shon, J. Ceram. Process. Res. 16[3] (2015) 346-351.
11. N.M. Parikh and M.JR. Humenik, J. Am. Ceram. Soc. 40[9] (1957) 315-320.
12. Y. Li, N. Liu, X. Zhang, and C. Rong, Int. J. Refract. Met. Hard Mater., 26[3] (2008) 190-196.
13. H.O. Andren, Mater. Des. 22[6] (2001) 491-498.
14. J. Song, Y. Liu, C. Pang, J. Zhang, L. Chen, X. Zhang, S. Guo, X. Wang, R. Wang, and A. Chen, J. Ceram. Process. Res. 19[2] (2018) 142-145.
15. S.H. Ko, W.S. Lee, J.M. Jang, B.H. Cha, and J.S. Seo, J. Ceram. Process. Res. 13[S1] (2012) 105-109.
16. C. Suryanarayana, Research 2019 (2019) 1-17.
17. A.I. Gusev and A.S. Kurlov, Nanotechnology 19 [26] (2008) 265302.
18. I. Topcu, J. Ceram. Process. Res. 22[3] (2021) 276-282.
19. E. S. Lee, S. K. Park and Y. H. Park, J. Ceram. Process. Res. 16[4] (2015) 380-384.
20. J. Hernandez, J. Zarate and G. Rosas, J. Ceram. Process. Res. 10[2] (2009) 144-147.
21. H. Hosokawa, K. Kato, K. Shimojima, and A. Matsumoto, Mater. Trans. 50[1] (2009) 117-122.
22. M. Bouleghlem, M. Zahzouh, M. Hamidouche, A. Boukhobaz, and M. Fellah, Int. J. Eng. Res. Africa 45 (2019) 1-14.
23. V.D. Mote, Y. Purushotham, and B.N. Dole, J. Theoretical and Appl. Phys. 6 (2015) 6.
24. B. Poon, D. Rittel, and G. Ravichandran, Int. J. Solids and Structures 45[24] (2008) 6018-6033.
25. D. Bandyopadhyay, B. Haldar, R.C. Sharma, and N. Carkraborti, J. Phase of Equilibria 20[3] (1999) 332-336.
26. W. Acchar and C.A. Cairo, Mat. Res. 9[2] (2006) 171-174.
27. N. Loudjani, N. Bensebaa, L. Dekhil, S. Alleg, and J.J. Sunol, J. Magnetism and Magnetic Mater. 323[23] (2011) 3063-3070.
28. S. Han, L. Zhao, Q. Jiang, and J. Lian, Sci. Reports 2 (2012) 493.
29. H. Dutta, A. Sen, J. Bhattaharjee, and S.K. Pradhan, J. Alloys, and Compd. 493[1-2] (2010) 666-671.
30. J.H. Lee, I.H. Oh, J.H. Jang, J.H. Kim, S.K. Hong, and H.K. Park, Met. Mater. Int. 9[2] (2020) 2247-2258.
31. S. Jia, A.J. Williams, P.W. Stephens, and R.J. Cava, Phys. Rev. B 80 (2009) 165107.
32. M.E. Sherif, J. Saida, and A. Inoue, Acta Mater. 50[10] (2002) 2725-2736.
33. F. Zhou, X. Liao, Y.T. Zhu, S. Dallek, and E. Lavernia, Acta Mater. 51[10] (2003) 2777-2791.
34. L. Boatemaa, J.C. Brouwer, S. van der Zwaag, and W.G.

Sloof, J. Mater. Sci. 53 (2018) 5973-5986.
35. W. Cao, O.K. Tan, W. Zhu, and B. Jiang, J. Solid State Chem. 155[2] (2000) 320-325.
36. Y. Peng, H. Miao, and Z. Peng, Int. J. Refrac. Metals and Hard Mater. 39 (2013) 78-89.
37. J.H. Lee, H.K. Park, J.H. Jang, S.K. Hong, and I.H. Oh, J. Alloys and Compd. 797 (2019) 612-621.
38. M. Toozandehjani, K.A. Matori, F. Ostovan, S.A. Aziz, and Md. S. Marmat, Materials 10[1] (2017) 1232.
39. C. Wang, D. Shi, and S. Li, Materials 13[5] (2020) 1256.
40. A. Bachmaier, M. Kerber, D. Setman, and R. Pippen, Acta Materialia 60[3] (2012) 860-871.
41. H. Kimura and T. Masumoto, J. Non Crystalline Solids 61-62 (1984) 835-839.